1   Theory of Elementary Particles

M. Bordone, S. Borowka, F. Buccioni, D. Buttazzo, L. Cieri, S. Devoto, T. Gehrmann,
M. Grazzini, N. Greiner, A. Greljio, C. Hanga, D. Hulme, A. Ilnicka, G. Isidori, T. Jezo,
D. Kara, A. Karlberg, J. Lindert, A. Lopresti, P. Lowdon, D. Marzocca, J. Mazzitelli,
N. Moretti, D. Müller, J. Niehues, G. Oeztürk, A. Pattori, S. Pozzorini, H. Sargsyan,
M. Schönherr, A. Signer, S. Trifinopoulos, Y. Ulrich, D. van Dyk, A. Visconti,
M. Wiesemann, D. Wyler, M. Zoller

in collaboration with: RWTH Aachen, CERN, IMSc Chennai, TU Dresden, Durham University, INFN Firenze,
Freiburg University, INFN and University of Genova, DESY Hamburgh, University of Lyon, Stephan Insistue
Ljubljana, Mainz University, Michigan State University, University of Milano Bicocca, MPI Munich, LPT
Orsay, INFN and University of Padova, Peking University, University of San Martin, Siegen University, SLAC
Stanford, IFIC Valencia, ETH Zürich.

The particle theory group at the Physik-Institut works on a broad spectrum of research projects related to the interpretation of data from high energy particle colliders. These cover precision calculations of benchmark observables, simulation of full collider events, identification of optimal observables for searches and measurements, physics beyond the Standard Model, as well as developments of calculational techniques. We summarize some highlights of last year's research below.

1.1 Next-to-leading order QCD predictions for top-quark pair production with up to three jets

The top quark as the heaviest known elementary particle plays a fundamental role, both in the Standard Model and in new physics scenarios. Experimental analyses of Large Hadron Collider (LHC) data collected during run II will provide unprecedented reach at high energy and in exclusive phase space regions with associated production of jets and vector bosons or Higgs bosons. The production of a $t\bar{t}$ system in association with multiple jets plays an especially important role as a background to new physics searches and to various Higgs and Standard Model analyses. In particular, the precise theoretical control of $t\bar{t}$+multijet backgrounds is one of the most important prerequisites for the observation of top-quark production in association with a Higgs boson, which would give direct access to the top-quark Yukawa coupling.

In this context, it is crucial to dispose of next-to-leading order (NLO) QCD predictions for $t\bar{t}$ production in association with the highest possible number of extra jets. However, the technical complexity of such calculations grows extremely fast with the number N_{jets} of extra jets. This is illustrated in Table 1.1, which lists

the number of one-loop Feynman diagrams that contribute to a few representative partonic channels as a function of N_{jets}. At $N_{\text{jets}} > 1$ the level of complexity starts to be very high, and the first NLO calculations for $pp \rightarrow t\bar{t} + 2\,\text{jets}$ [1–3] belong to the breakthroughs of the so-called NLO revolution. Very recently we have present the first NLO results for $t\bar{t} + 3\,\text{jets}$. At present only few scattering processes with more than four final-state particles are known at NLO, and the calculation at hand is the first one that deals with a $2 \rightarrow 5$ process with seven colored external particles including also heavy quarks. These results could be achieved thanks to OPENLOOPS [4, 5], an automated generator of one-loop matrix elements that was developed in the recent years at our institute. It allows to perform multi-particle NLO calculations with remarkably high efficiency.

In [6] we have presented a series of NLO calculations for $pp \rightarrow t\bar{t} + 0, 1, 2, 3\,\text{jets}$ at the 13 TeV LHC. Exploiting the unprecedented reach in jet multiplicity, we have studied the scaling behavior in N_{jets}, and we have shed new light on the general issue of scale setting and theoretical scale uncertainties in the context of multi-scale processes.

TAB. 1.1 – Number of one-loop Feynman diagrams in representative partonic channels in $pp \rightarrow t\bar{t} + N\,\text{jets}$ for $N = 0, 1, 2, 3$.

partonic channel \ N	0	1	2	3
$gg \rightarrow t\bar{t} + N\,g$	47	630	9'438	152'070
$u\bar{u} \rightarrow t\bar{t} + N\,g$	12	122	1'608	23'835
$u\bar{u} \rightarrow t\bar{t}u\bar{u} + (N-2)\,g$	–	–	506	6'642
$u\bar{u} \rightarrow t\bar{t}d\bar{d} + (N-2)\,g$	–	–	252	3'321

The multiple scales that enter $t\bar{t}+$ multijet cross sections and distributions can be distributed over more than two orders of magnitude. In this situation, finding renormalization (μ_R) and factorization (μ_F) scales that ensure a decent convergence of perturbative QCD for the widest possible range of observables is not trivial. Moreover, in the presence of a wide spectrum of scales, the standard approach of using factor-two scale variations for the estimation of theoretical uncertainties due to missing higher-order effects becomes questionable. Motivated by these observations, to gain more insights into the scale dependence of $t\bar{t}+$ multijet production and related uncertainties we have compared the standard approach of using a hard scale choice ($\mu = H_T/2$), against the MINLO method [7]. The latter can be regarded as an optimal scale-setting approach for multi-scale processes, as it resums soft and collinear logarithms that emerge in the presence of large ratios of scales. Our study provides the first systematic comparison of these two approaches.

As an illustration of our results, we show in Fig. 1.1 the jet multiplicity distribution for $t\bar{t} + 0, 1, 2, 3$ jets. The top panel displays four predictions, stemming from fixed-order LO and NLO calculations, and from MINLO computations at LO and NLO (labeled 'MILO' and 'MINLO'). The second panel shows the ratio between LO and NLO predictions at fixed order, while the third panel shows the ratio between MILO and MINLO predictions. The last panel shows the ratio between MINLO and NLO. The bands illustrate scale uncertainties estimated through independent factor-two rescaling of μ_R and μ_F. Fixed-order predictions feature rather large NLO corrections of about $+50\%$ for all jet multiplicities, while MINLO results feature steadily decreasing corrections for increasing N_{jets}. In both cases, LO scale uncertainties tend to grow by more than 10% at each extra jet emission, while (MI)NLO scale uncertainties are significantly reduced, and the total width of the (MI)NLO variation bands is about 20–25% for all considered N_{jets} values. Comparing fixed-order NLO and MINLO predictions we observe a remarkable agreement at the level of 4–8%. This supports NLO and MINLO scale-uncertainty estimates based on factor-two variations.

In general, for a wide wide range of observables at the 13 TeV LHC, we found remarkably good agreement between the predictions generated at fixed order and with the MINLO method [6]. More precisely, MINLO cross sections tend to feature a better perturbative convergence and to lie systematically above NLO ones. But the differences turn out to be well consistent with factor-two scale variations of the respective predictions. These findings significantly extend and consolidate the conventional picture of theoretical uncertainties that results from standard scale choices and scale variations. The anticipated level of theoretical precision for $t\bar{t}+$ multijet production is at the level of ten percent or better.
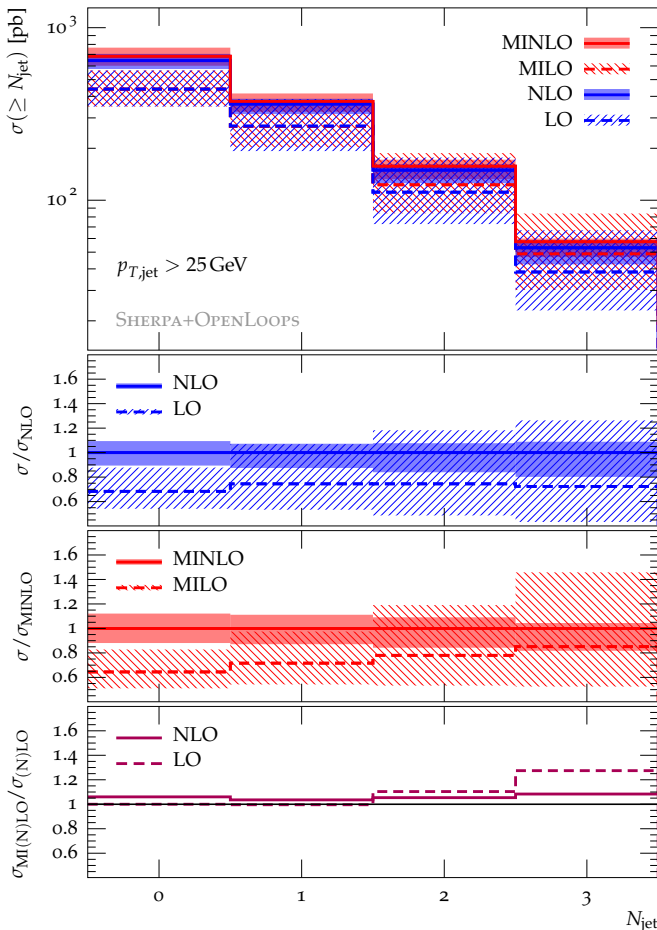

FIG. 1.1 – Inclusive $t\bar{t}+$ multijet cross sections at the 13 TeV LHC with a minimum number $N = 0, 1, 2, 3$ of jets at $p_{T,\mathrm{jet}} \geq 25$ GeV.

[1] A. Bredenstein, A. Denner, S. Dittmaier, and S. Pozzorini, Phys. Rev. Lett. **103** (2009) 012002.

[2] F. Cascioli, P. Maierhöfer, N. Moretti, S. Pozzorini, and F. Siegert, Phys. Lett. **B734** (2014) 210-214.

[3] S. Höche, F. Krauss, P. Maierhöfer, S. Pozzorini, M. Schönherr, and F. Siegert, Phys. Lett. **B748** (2015) 74-78.

[4] F. Cascioli, P. Maierhöfer, and S. Pozzorini, Phys. Rev. Lett. **108** (2012) 111601.

[5] F. Cascioli, J. Lindert, P. Maierhöfer, and S. Pozzorini, *The OpenLoops one-loop generator*, publicly available at http://openloops.hepforge.org.

[6] S. Höche, P. Maierhöfer, N. Moretti, S. Pozzorini, and F. Siegert, Eur. Phys. J. **C77** (2017), no. 3 145

[7] K. Hamilton, P. Nason, and G. Zanderighi, JHEP **1210** (2012) 155.

1.2 $W^{\pm}Z$ production at NNLO

The production of a pair of vector bosons is among the most relevant physics processes at LHC. Besides playing a central role in precision tests of the gauge structure of electroweak (EW) interactions and in studies of the mechanism of EW symmetry breaking, vector-boson pair production constitutes an irreducible background in most of the Higgs-boson measurements and in many searches for physics beyond the Standard Model (SM). The Tevatron collaborations have measured cross sections for vector-boson pair production at invariant masses larger than those probed at LEP2, setting limits on the corresponding anomalous couplings, and the LHC experiments are now continuing this research program and delivering results with increasing accuracy.

In the following we focus on $W^{\pm}Z$ production, which offers a valuable test of the triple gauge-boson couplings, and is an important SM background in many searches. We present next-to-next-to-leading order (NNLO) theoretical predictions [8] for this process at the LHC and compare them with the ATLAS and CMS data. The required tree-level and one-loop amplitudes were obtained with the OPENLOOPS [9] generator, which employs the Denner-Dittmaier algorithm for the numerical evaluation of one-loop integrals and implements a fast numerical recursion for the calculation of NLO scattering amplitudes within the SM. The two-loop amplitudes are taken from [10]. The required amplitudes are infrared divergent and are combined by using the q_T subtraction method [11] as implemented in the numerical program MATRIX.

In the following we present predictions for proton–proton collisions with $\sqrt{s} = 7, 8, 13$ and 14 TeV, setting the central scales μ_R and μ_F to $\mu_R = \mu_F = \mu_0 \equiv \frac{1}{2}(m_Z + m_W) = 85.7863$ GeV. Scale uncertainties are obtained by independently varying μ_R and μ_F in the range $0.5\mu_0 \le \mu_R, \mu_F \le 2\mu_0$ with the constraint $0.5 \le \mu_R/\mu_F \le 2$. The cross section results are always summed over the electrical charges of the final-state W bosons.

We first present results for the ATLAS definition of the $W^{\pm}Z$ cross sections, reported in Tab. 1.2, where we compare with the 7 and 8 TeV ATLAS measurements of Ref. [12] and Ref. [13], respectively. The relative impact of radiative corrections ranges between 63% and 83% at NLO and between 8% and 11% at NNLO for the collider energies under consideration.

In contrast to ZZ and WW production, in the case of $W^{\pm}Z$ the $\mathcal{O}(\alpha_S^2)$ corrections are genuine NNLO corrections to the $q\bar{q}$ channel. Since the $W^{\pm}Z$ final state is electrically charged, the production process does not receive contributions from a loop-induced gluon-fusion channel. The rather large impact of radiative corrections is due to the existence of a *radiation zero* in the Born scattering amplitudes. More precisely, the partonic on-shell Born $W^{\pm}Z$ amplitude exhibits an *approximate* radiation zero, which is broken by real corrections starting from NLO, thereby leading to a large impact of radiative corrections.

The perturbative uncertainties, estimated via scale variations, drop from about $\pm 5\%$ at NLO to about $\pm 2\%$ at NNLO. In particular, the impact of NNLO corrections is larger than anticipated from NLO scale variations. The large size of QCD radiative corrections is due to an approximate radiation zero which is present in the on-shell amplitude at LO. Since all partonic channels are included at NNLO, and the NNLO corrections, although significant, are still much smaller than the NLO effects, we expect that scale variations should provide the correct order of magnitude of the uncertainty from yet uncalculated higher-order contributions beyond NNLO.

Comparing with the experimentally measured cross sections [12, 13], we find that the inclusion of NNLO corrections clearly improves the agreement between data and theory, in particular at 8 TeV, where the measurement is most precise. While the central NLO prediction is roughly 2σ away from the measured cross section at 8 TeV, the NNLO prediction is right on top of the data with fully overlapping uncertainty bands.

Next, we provide theory predictions for the $W^{\pm}Z$ cross sections as defined by CMS in Tab. 1.3, where

TAB. 1.2 – Total cross sections with ATLAS mass window $66\,\text{GeV} < m(Z) < 116\,\text{GeV}$ at LO, NLO and NNLO. The available ATLAS data from Refs. [12, 13] are also shown.

$\sqrt{s}$ [TeV]	σ_{LO} [pb]	σ_{NLO} [pb]	σ_{NNLO} [pb]	σ_{ATLAS} [pb]
7	$11.028(8)^{+0.5\%}_{-1.2\%}$	$17.93(1)^{+5.3\%}_{-4.1\%}$	$19.34(3)^{+1.6\%}_{-1.8\%}$	$19.0^{+1.4}_{-1.3}(\text{stat})^{+0.9}_{-0.9}(\text{syst})^{+0.4}_{-0.4}(\text{lumi})$
8	$13.261(9)^{+1.3\%}_{-2.1\%}$	$22.03(2)^{+5.1\%}_{-3.9\%}$	$23.92(3)^{+1.7\%}_{-1.8\%}$	$24.3^{+0.6}_{-0.6}(\text{stat})^{+0.6}_{-0.6}(\text{syst})^{+0.5}_{-0.5}(\text{lumi})^{+0.4}_{-0.4}(\text{theo})$
13	$24.79(2)^{+4.2\%}_{-5.2\%}$	$44.67(3)^{+4.9\%}_{-3.9\%}$	$49.62(6)^{+2.2\%}_{-2.0\%}$	
14	$27.14(2)^{+4.7\%}_{-5.7\%}$	$49.50(3)^{+4.9\%}_{-4.0\%}$	$55.10(7)^{+2.3\%}_{-2.0\%}$	

TAB. 1.3 – Total cross sections with CMS mass windows of 71 GeV $< m(Z) <$ 111 GeV for 7 and 8 TeV, and 60 GeV $< m(Z) <$ 120 GeV for 13 and 14 TeV, at LO, NLO and NNLO. The available CMS data from Refs. [14, 15] are also shown.

$\sqrt{s}$ [TeV]	σ_{LO} [pb]	σ_{NLO} [pb]	σ_{NNLO} [pb]	σ_{CMS} [pb]
7	$10.902(7)^{+0.5\%}_{-1.2\%}$	$17.72(1)^{+5.3\%}_{-4.1\%}$	$19.18(3)^{+1.7\%}_{-1.8\%}$	$20.76^{+1.32}_{-1.32}(\text{stat})^{+1.13}_{-1.13}(\text{syst})^{+0.46}_{-0.46}(\text{lumi})$
8	$13.115(9)^{+1.3\%}_{-2.1\%}$	$21.80(2)^{+5.1\%}_{-3.9\%}$	$23.68(3)^{+1.8\%}_{-1.8\%}$	$24.61^{+0.76}_{-0.76}(\text{stat})^{+1.13}_{-1.13}(\text{syst})^{+1.08}_{-1.08}(\text{lumi})$
13	$25.04(2)^{+4.3\%}_{-5.3\%}$	$45.09(3)^{+4.9\%}_{-3.9\%}$	$49.98(6)^{+2.2\%}_{-2.0\%}$	$40.9^{+3.4}_{-3.4}(\text{stat})^{+3.1}_{-3.3}(\text{syst})^{+1.3}_{-1.3}(\text{lumi})^{+0.4}_{-0.4}(\text{theo})$
14	$27.39(2)^{+4.7\%}_{-5.7\%}$	$49.91(4)^{+4.9\%}_{-4.0\%}$	$55.60(7)^{+2.3\%}_{-2.0\%}$	

we also quote the results of the CMS measurements performed at 7 [14] and 8 [15] TeV . The slightly different definition of the Z-mass window as compared to ATLAS has only a very mild impact on the cross section. In particular, both the relative size of higher-order corrections and the bands obtained by scale variation are almost identical to the ones obtained with the ATLAS definition. Comparing with the measured cross sections, we again find excellent agreement between our NNLO predictions and the cross sections reported by CMS for $\sqrt{s} = 7$ and 8 TeV, where the inclusion of NNLO corrections clearly improves the agreement, in particular at 8 TeV. The measurement at 13 TeV undershoots the NNLO prediction, being consistent with it only at the level of about 2σ. However, at this early stage of LHC Run 2, the measurement still comes with quite large experimental uncertainties of both systematical and statistical nature, and the measured cross section might still be subject to a significant shift with respect to its central value, once statistics increases. Fig. 1.2 shows a summary plot where we compare NLO and NNLO predictions to all available LHC measurements of the total $W^\pm Z$ cross section.
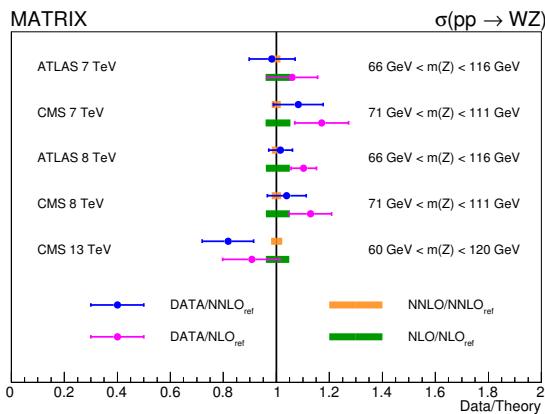

FIG. 1.2 – Summary plot for comparison of NLO and NNLO predictions with the available LHC measurements of the total $W^\pm Z$ cross section. Theory uncertainties are obtained through scale variations as described in the text.

[8] M. Grazzini, S. Kallweit, D. Rathlev, and M. Wiesemann, Phys. Lett. **B761** (2016) 179-183.

[9] F. Cascioli, P. Maierhofer, and S. Pozzorini, Phys. Rev. Lett. **108** (2012) 111601.

[10] T. Gehrmann and L. Tancredi, JHEP **02** (2012) 004.

[11] S. Catani and M. Grazzini, Phys. Rev. Lett. **98** (2007) 222002.

[12] G. Aad et al. [ATLAS collaboration], Eur. Phys. J. **C72** (2012) 2173.

[13] G. Aad et al. [ATLAS collaboration], Phys. Rev. **D93** (2016), no. 9 092004.

[14] CMS Collaboration, CMS-PAS-SMP-12-006.

[15] CMS Collaboration, CMS-PAS-SMP-16-002.

1.3 NNLO QCD corrections to jet production in deep inelastic scattering

Hadronic jets in deeply inelastic electron-proton collisions are produced by the scattering of a parton from the proton with the virtual gauge boson mediating the interaction. The HERA experiments have performed precision measurements of inclusive single jet production and di-jet production in the Breit frame, which provide important constraints on the strong coupling constant and on parton distributions in the proton. We recently completed the calculation of the NNLO QCD corrections to these processes [16].

The QCD corrections at this order involve three types of scattering amplitudes: the two-loop amplitudes for two-parton final states, the one-loop amplitudes for three-parton final states and the tree-level amplitudes for four-parton final states. The contribution from each partonic final state multiplicity contains infrared divergences from soft and collinear real radiation and from virtual particle loops; these infrared singularities cancel only once the different multiplicities are summed together for any infrared-safe final state definition. To implement the
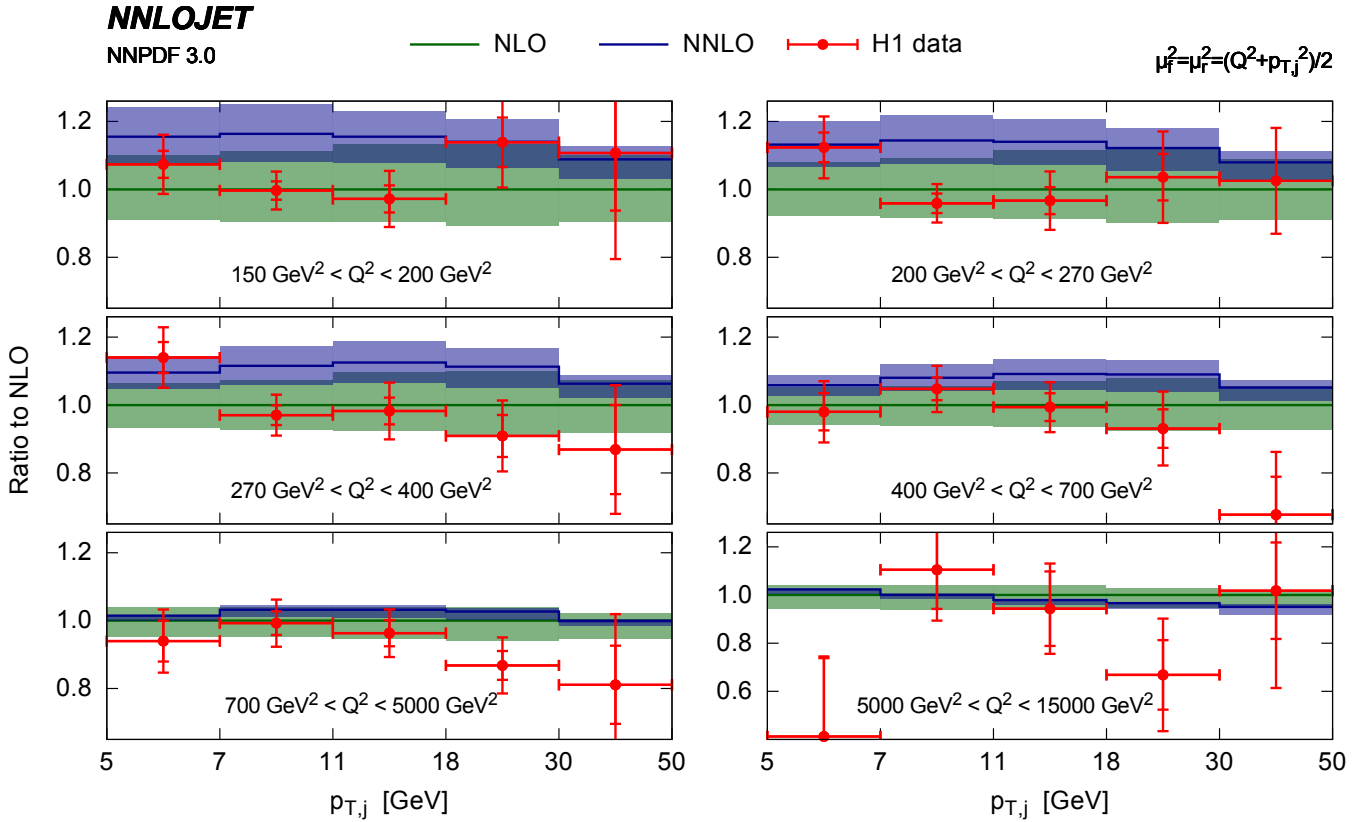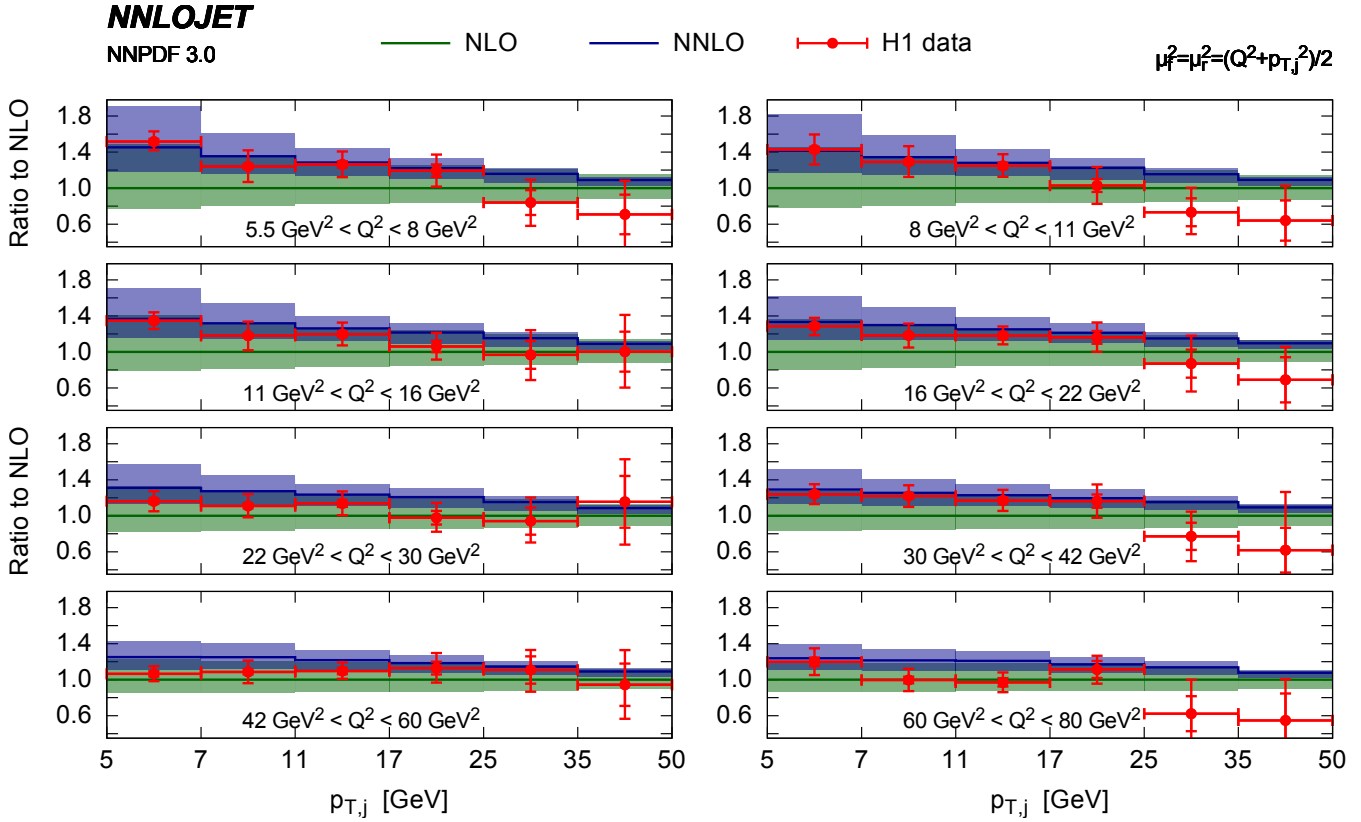
FIG. 1.3 – Inclusive jet production cross section as a function of the jet transverse momentum $p_{T,B}$ in bins of Q^2, compared to H1 data [22].

different contributions into a numerical program, a procedure for the extraction of all infrared singular configurations from each partonic multiplicity is needed. Our calculation is based on the antenna subtraction method [17], which constructs the subtraction terms for the real radiation processes out of antenna functions that encapsulate all color-ordered unresolved parton emission in between a pair of hard radiator partons, multiplied with reduced matrix elements of lower partonic multiplicity. By factorizing the final state phase space accordingly, it is possible to analytically integrate the antenna functions to make their infrared pole structure explicit, such that the integrated subtraction terms can be combined with the virtual corrections to yield a finite result. The combination of real radiation contributions and unintegrated antenna subtraction terms is numerically finite in all infrared limits, such that all parton-level contributions to two-jet final states at NNLO can be implemented into a numerical program (parton-level event generator). This program can then incorporate the jet algorithm used in the experimental measurement as well as any type of event selection cuts. A substantial part of the infrastructure of our program is common to other NNLO calculations of jet production observables within the antenna subtraction method [18–21], which are all part of a newly developed code named NNLOJET.

Inclusive jet production in deep inelastic scattering has been widely studied by the H1 and ZEUS experiments at DESY HERA. The jet measurements are performed in the Breit frame, where the transverse momentum requirement on the jet ensures the existence of a partonic recoil, even if only a single jet is reconstructed in the kinematical acceptance.

Figure 1.3 compares our NNLO predictions to the H1 data. We observe that the NNLO corrections are very substantial at low-Q^2 and low-p_T^B, with an up to 60% enhancement with respect to NLO. These large corrections are within the NLO uncertainty band (close to the upper edge), and result in a residual theory uncertainty of 20% even at NNLO. Especially at low Q^2, the shape and normalization of the theory prediction changes significantly going from NLO to NNLO, and results in a considerably improved theoretical description of the data, as statistically quantified in the experimental H1 study [22]. With increasing Q^2, the size of the NNLO corrections decreases, accompanied with very small residual theoretical uncertainties (decreasing from 10% at $Q^2 = 150$ GeV^2 to 2% at 5000 GeV^2). In this region, the combination of precision data with the newly derived NNLO corrections has clearly the potential to provide important new constraints for precision QCD studies.

[16] J. Currie, T. Gehrmann, and J. Niehues, Phys. Rev. Lett. **117** (2016), no. 4 042001.

[17] A. Gehrmann-De Ridder, T. Gehrmann, and E. W. N. Glover, JHEP **09** (2005) 056.

[18] A. Gehrmann-De Ridder, T. Gehrmann, E. W. N. Glover, A. Huss, and T. A. Morgan, Phys. Rev. Lett. **117** (2016), no. 2 022001.

[19] A. Gehrmann-De Ridder, T. Gehrmann, E. W. N. Glover, A. Huss, and T. A. Morgan, JHEP **07** (2016) 133.

[20] X. Chen, J. Cruz-Martinez, T. Gehrmann, E. W. N. Glover, and M. Jaquier, JHEP **10** (2016) 066.

[21] A. Gehrmann-De Ridder, T. Gehrmann, E. W. N. Glover, A. Huss, and T. A. Morgan, JHEP **11** (2016) 094.

[22] V. Andreev *et al.* [H1 collab.], Eur. Phys. J. **C77** (2017), no. 4 215.

1.4 Charged Lepton-Flavor Violation

While it is by now well established that lepton flavor is not conserved in the neutral sector (neutrinos), so far there is no experimental evidence for lepton-flavor violation in the charged sector. Within the SM such processes have a branching ratio $\mathcal{B}$ that is much too small to be detected in any foreseeable experiment. Hence, any experimental signature of charged lepton-flavor violation (cLFV) is a clear signal for physics beyond the SM.

At the Paul Scherrer Institute (PSI) there are experiments ongoing and planned to improve the sensitivity in cLFV searches in two golden channels, namely $\mu \to e\gamma$ by MEG [23] and $\mu \to 3e$ by Mu3e [24]. One of the many issues that these experiments are faced with is the irreducible background of SM processes with very low-energy neutrinos. In the case of Mu3e, the SM process $\mu^+ \to e^+(e^+e^-)\nu_e\bar{\nu}_\mu$ cannot be distinguished from the signal if the invisible energy $\not{E} \equiv E(\nu_e) + E(\bar{\nu}_\mu)$ tends to zero. Hence it is important to have reliable predictions of this SM process. In Ref. [25] we have presented a fully differential computation at next-to-leading order in the electromagnetic coupling α. As an illustration, in the left panel of Fig. 1.4 we show the $\not{E}$ spectrum, taking into account cuts on the final state electrons that mimic the Mu3e detector. The corrections turn out to be negative and amount to about -15% for $\not{E} \lesssim 3$ MeV. Thus, there are considerably fewer background events than anticipated from a leading-order computation.

Apart from studying background events for the cLFV experiments at PSI, we have also analyzed [26] the complementarity of these experiments, using an effective-theory approach with dimension 6 operators to describe physics beyond the SM. As an example, in the right panel of Figure 1.4 we compare the constraining power of MEG, Mu3e and future electron conversion experiments (e.g. COMET) on C_L^D and C_{ee}^{VRR}, the Wilson coefficients of the
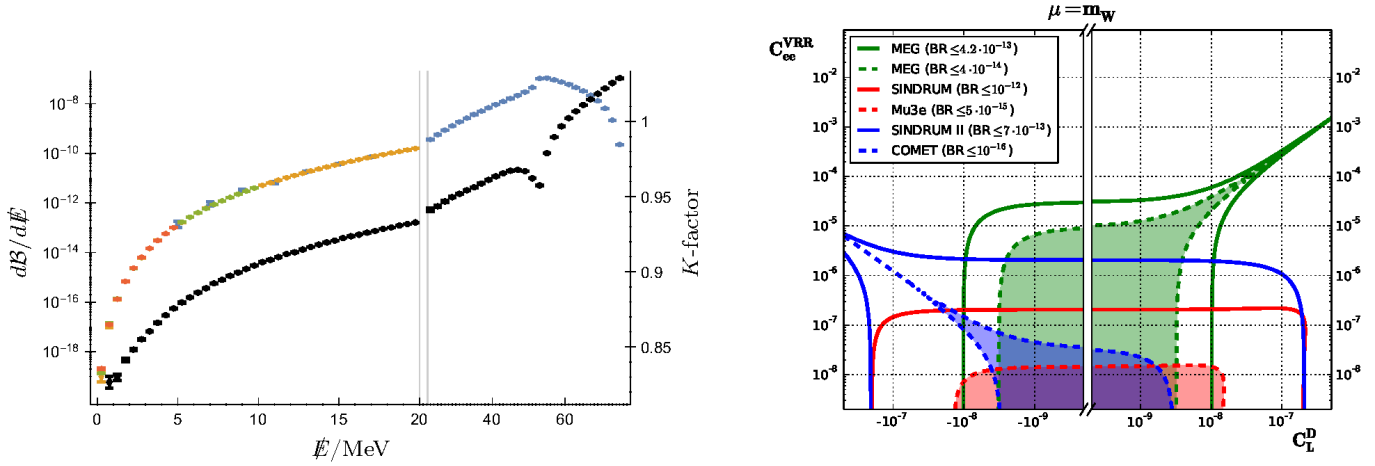
FIG. 1.4 – Left panel: invisible energy spectrum of the process $\mu^+ \to e^+(e^+e^-)\nu_e\bar{\nu}_\mu$ at NLO, taking into account the geometry of the future Mu3e detector. Right panel: Comparison of sensitivity on the Wilson coefficients C_L^D and C_{ee}^{VRR} from various cLFV experiments.

dipole operator and a four-fermion operator, respectively. The main feature of this example extends to many other Wilson coefficients: the various cLFV experiments complement each other in that they are most sensitive to different scenarios of beyond the SM physics.

[23] A. M. Baldini *et al.* [MEG Collaboration], Eur. Phys. J. **C76** (2016), no. 8 434

[24] A. Blondel *et al.*, arXiv:1301.6113.

[25] G. M. Pruna, A. Signer, and Y. Ulrich, Phys. Lett. **B765** (2017) 280-284.

[26] A. Crivellin, S. Davidson, G. M. Pruna, and A. Signer, arXiv:1702.0302.

1.5 Flavor physics within and beyond the SM

In the last few years the indirect search for physics beyond the Standard Model (SM) in the flavor sector has become particularly interesting in view of a series of experimental "anomalies" in B decays. Although their statistical significance is still limited, these anomalies indicate possible violations of Lepton Flavor Universality (LFU) both in charged- and in neutral-current semi-leptonic B decays. Motivated by these observations, we have analyzed various aspects of LFU, both from a pure phenomenological perspective and in the context of motivated extensions of the SM. Our research has been articulated along three main directions.

- *SM predictions for LFU tests*.
  In Ref. [27] we have have presented the first reliable

SM predictions of two of the key observables used to test LFU in neutral-current B decays, namely the ratios $R_K = \Gamma[B \to K\mu^+\mu^-]/\Gamma[B \to Ke^+e^-]$ and $R_{K^*} = \Gamma[B \to K^*\mu^+\mu^-]/\Gamma[B \to K^*e^+e^-]$. We have shown that, within the SM, these ratios differ by 1 by at most $\pm 1\%$ (for $m_{\ell\ell} > 1$ GeV), offering a very clean probe of physics beyond the Standard Model.

- *New physics analyses based on Effective Theory approaches and simplified models*.
  In 2015 our group has demonstrated, for the first time, the possibility of a coherent explanation of both charged- and neutral-current LFU anomalies, namely i) the breaking of τ–μ universality in $B \to D^{(*)}\ell\nu$ decays; ii) the breaking of μ–e universality in $B \to K\ell^+\ell^-$ decays. Such combination is highly non-trivial due to severe constraints from other observables, both at low- and high-energies. Continuing along this research direction, we have further investigated such bounds [28–31] using both Effective Field Theory (EFT) approaches and simplified dynamical models. The result of our analysis is that a combined explanation of these effects require some moderate tuning (in the EFT parameter space) but is still possible. A general prediction resulting from a combined explanation of these anomalies is the expectation of sizeable deviations from the SM in $pp \to X + \tau^+\tau^-$ (for large $m_{\tau\tau}$) within the reach of future ATLAS and CMS searches.
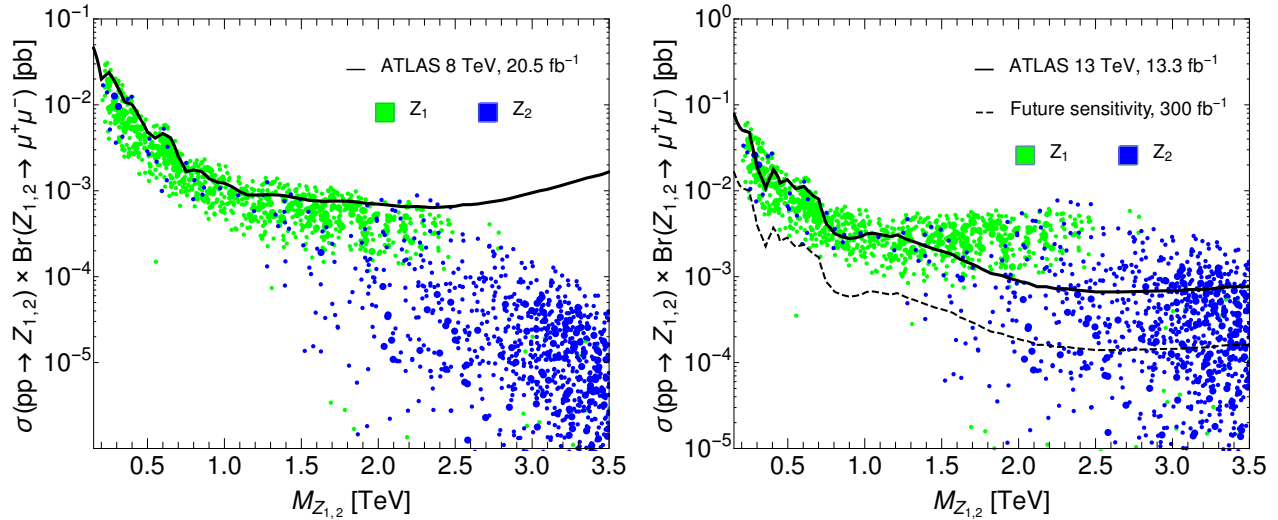
FIG. 1.5 – Predictions for the LHC signals ($\sigma \times \mathcal{B}$) at 8 TeV (left) and 13 TeV (right) for $\mu^+\mu^-$ resonance searches for the leptophilic Z_1 (green) and the leptophobic Z_2 (blue) states predicted in the model of Ref. [32], based on dynamical Yukawa couplings and addressing B-physics anomalies. Present limits are shown with black line, and future-projected with dashed line.

- *UV completions.*

The last research line is the attempt to find motivated UV completions for the simplified models addressing these anomalies. In 2016 we identified two interesting examples of UV completions: i) a model based on a gauged non-Abelian flavor symmetry (motivated by a dynamical explanation of quark and lepton Yukawa couplings) [32]; ii) a class of models based on vector-like confinement (motivated by a solution to the hierarchy problem) [33]. In both cases we have exploited the signatures of such models at high-p_T, in view of future searches by ATLAS and CMS (see e.g. Fig. 1.5).

[27] M. Bordone, G. Isidori, and A. Pattori, Eur. Phys. J. **C76** (2016), no. 8 440.

[28] F. Feruglio, P. Paradisi, and A. Pattori, Phys. Rev. Lett. **118** (2017), no. 1 011801.

[29]] D. A. Faroughy, A. Greljo, and J. F. Kamenik, Phys. Lett. **B764** (2017) 126-134.

[30] C. Biggio, M. Bordone, L. Di Luzio, and G. Ridolfi, JHEP **10** (2016) 002.

[31] M. Bordone, G. Isidori, and S. Trifinopoulos, arXiv:1702.0723.

[32] A. Crivellin, J. Fuentes-Martin, A. Greljo, and G. Isidori, Phys. Lett. B766 (2017) 77-85.

[33] D. Buttazzo, A. Greljo, G. Isidori, and D. Marzocca, JHEP 08 (2016) 035.